subsonic turbulent boundary layer is typically 0.021. This produced an $f_v = 5.34$ kHz, which is within 53.8% of Rossiter's predicted edgetones for the $m = 1$ mode.

As previously noted, an examination of the present frequency spectra at 0-deg yaw clearly indicated 22.75 kHz as the fundamental mode, with secondary peaks between 120 and 350 Hz. Because the fundamental mode matches the acoustic mode f_D within 2%, it may be suggested that the dominant oscillation was the result of a transverse mode. Therefore, the transverse acoustic mode based on the cavity depth would appear to be the mechanism producing the pressure oscillations recorded along the cavity floor and not the mode corresponding to vortex shedding. Yet, Rossiter's[5] second mode also agrees with the present measurements to within 1.7%, suggesting a fluid dynamic mechanism. In addition, the second mode is in good agreement with the computations of Tam et al.,[10] who determined this frequency numerically via an FFT of the pressure history at the wall centerline. Their computed frequency was approximately 26 kHz. Further, a recent work by the Ref. 12 authors provided flowfield simulations that contained a pressure wave that reflected off the floor of the cavity. This pressure wave may represent the transverse acoustic mode.

Although a combined fluid resonant flow may be the logical conclusion, it is suggested that the acoustic mode, which produced a self-sustaining oscillation in spite of small geometric changes, may be the dominant driving mechanism in the present study, at least until ψ of 35 deg. This result is similar to the flow transition reported by Zhang and Edwards[13] in which the flow switched modes from a transverse oscillation to a longitudinal oscillation as the cavity length was increased. In the present study, mode switching between 35 and 45 deg was observed to produce oscillations with frequencies of either 23 or 3.5 kHz. Beyond 45 deg, a permanent mode switch was observed. The resultant dominant frequency was 7.7 kHz at 45 deg, which increased linearly to 12.5 kHz at 65 deg yaw.

Summary

An investigation into the effect of yaw angle variations in a two-dimensional open cavity placed within a supersonic freestream was performed. The effect of yaw angle changes on the frequency of the dominant pressure oscillation was noted. Specifically, there appeared to be little change in the frequency of the oscillation up to 37.5 deg. Comparison of the measured dominant mode to the fundamental acoustic mode based on cavity depth, i.e., the transverse mode, were found to be in excellent agreement. This suggests that the dominant mechanism for the present configuration was acoustic in nature and not fluid dynamic. However, a variation in the secondary mode, probably fluid dynamic in nature, showed an increased importance as the yaw angle was increased.

Acknowledgments

The authors wish to thank Leonidas Sakell and the Air Force Office of Scientific Research for their generous support through Grant F49620-93-0081. The authors also appreciate the engineering support of Curtis Fox.

References

[1]Krishnamurty, K., "Acoustic Radiation from Two-Dimensional Rectangular Cutouts in Aerodynamic Surfaces," NACA TN-3487, Aug. 1955.

[2]Charwat, A. F., Roos, J. N., Dewey, C. F., and Hitz, J. A., "An Investigation of Separated Flows—Part I: The Pressure Field," *Journal of the Aerospace Sciences*, Vol. 28, No. 6, 1961, pp. 457–470.

[3]Charwat, A. F., Roos, J. N., Dewey, C. F., and Hitz, J. A., "An Investigation of Separated Flows—Part II: Flow Separation in the Cavity and Heat Transfer," *Journal of the Aerospace Sciences*, Vol. 28, No. 7, 1961, pp. 513–527.

[4]Heller, H., and Bliss, D., "Aerodynamically Induced Pressure Oscillations in Cavities: Physical Mechanisms and Suppression Concepts," U.S. Air Force Flight Dynamics Lab., AFFDL-TR-74-133, Dayton, OH, Feb. 1975.

[5]Rossiter, I. E., "Wind Tunnel Experiments on the Flow Field over Rectangular Cavities at Subsonic and Transonic Speeds," Aeronautical Research Council, Repts. and Memoranda No. 3438, Oct. 1964.

[6]Tracy, M. B., and Plentovich, E. B., "Characterization of Cavity Flow Fields Using Pressure Data Obtained in the Langley 0.3-Meter Transonic Cryogenic Tunnel," NASA TM 4436, March 1993.

[7]Tracy, M. B., Plentovich, E. B., and Chu, J.,"Measurements of Fluctuating Pressure in a Rectangular Cavity in Transonic Flow at High Reynolds Numbers," NASA TM 4363, June 1992.

[8]Plentovich, E. B., Chu, J., and Tracy, M. B., "Effect of Yaw Angle and Reynolds Number on Rectangular-Box Cavities at Subsonic and Transonic Speeds," NASA TP-3099, July 1991.

[9]Baysal, O., and Yen, G.-W., "Implicit and Explicit Computations of Flows Past Cavities With and Without Yaw," AIAA Paper 90-0049, Jan. 1990.

[10]Tam, C. J., Orkwis, P. D., and Disimile, P. J., "A Comparison of Several Turbulence Models for 2-D Open Cavity Flow Field Computations," AIAA Paper 95-0361, Jan. 1995.

[11]Plentovich, E. B., Stallings, R. L., Jr., and Tracy, M. B., "Experimental Cavity Pressure Measurements at Subsonic and Transonic Speeds: Static Pressure Results," NASA TP 3358, Dec. 1993.

[12]Tam, C. J., Orkwis, P. D., and Disimile, P. J., "Supersonic Open Cavity Flow Physics Ascertained from Algebraic Turbulence Model Simulations," AIAA Paper 96-0075, Jan. 1996.

[13]Zhang, X., and Edwards, J. A., "Experimental Investigation of Supersonic Flow over Two Cavities in Tandem," *AIAA Journal*, Vol. 30, No. 5, 1992, pp. 1182–1190.

P. R. Bandyopadhyay
Associate Editor

Computations of Unsteady Separating Flows over an Oscillating Airfoil

Sungho Ko* and W. J. McCroskey†
NASA Ames Research Center,
Moffett Field, California 94035-1000

Introduction

UNSTEADY separating flows over oscillating airfoils occur in many important engineering applications, such as airplanes, helicopter rotors in forward flight, and turbine blades. There are some distinct features of the unsteady separating flows (dynamic stall) over a rapidly oscillating airfoil that draw the special attention of many scientists. These features include large amounts of force and moment hysteresis and oscillatory pressure fluctuations. In most situations, these features of dynamic stall significantly limit the performance of the device.

The primary objective of the present study is to identify the most accurate, robust, and economic turbulence model for dynamic stall computations. However, testing all of the turbulence models available is simply impractical. Alternatively, only a few popular and representative models are selected after surveying papers and reports on separated flows. The Baldwin–Lomax (B–L) model[1] is selected because of its popularity as a zero-equation model. The Spalart–Allmaras (S–A) model[2] is chosen among one-equation models because of its excellent performance. Finally, the k–ϵ model[3] is selected because it is the most popular two-equation model.

Numerical Methods

The governing equations are the time-averaged, two-dimensional, compressible thin-layer Navier–Stokes equations. These governing equations are solved by the TURNS (Transonic Unsteady Rotor Navier–Stokes) code.[4] The inviscid convective fluxes $\hat{\boldsymbol{E}}$ and $\hat{\boldsymbol{G}}$ are differenced by the Roe's upwind-biased flux-difference splitting scheme.[5]

The time-marching integration of the governing equations is done by using the lower–upper symmetric Gauss–Seidel (LU-SGS) implicit scheme.[6] Whereas the LU-SGS scheme is unconditionally

Presented as Paper 95-0312 at the AIAA 33rd Aerospace Sciences Meeting, Reno, NV, Jan. 9–12, 1995; received Feb. 6, 1995; revision received March 11, 1997; accepted for publication March 21, 1997.

*Research Scientist, Sterling Federal Systems, Inc.; currently Assistant Professor, Department of Mechanical Design Engineering, Chungnam National University, Taejon 305-764, Korea. Member AIAA.

†Senior Research Scientist, U.S. Army Aeroflightdynamics Directorate–Aviation and Troop Command. Fellow AIAA.

stable and fast, it is limited to first-order accuracy in time. Therefore, Newton subiterations at each time step are used for unsteady flow computations in order to minimize errors arising from linearization and factorization.

The turbulent transport equations are decoupled from the mean flow equations and is solved by an implicit factored alternating direction implicit scheme.[7]

In dynamic stall computations, a two-dimensional, body-fitted C-type computational grid moves in a sinusoidal pitching motion about an airfoil's quarter chord in the inertial reference frame (x, z, t). At each time level the new location of the grid is computed, and all metrics and the Jacobian of the transformation are recalculated. To capture the freestream accurately, a modified finite volume method[8] is used for calculating both space and time metrics.

Results

Unsteady two-dimensional turbulent flows over an oscillating NACA 0015 airfoil have been computed using the selected three turbulence models. A wind-tunnel experiment conducted by Piziali[9] at the U.S. Army Aeroflightdynamics Directorate has been chosen for the test case.

The computations were done for a freestream Mach number M_∞ of 0.29 and a chord Reynolds number of 1.95×10^6. With a reduced frequency k equal to 0.1, the instantaneous angle of attack (degrees) of the pitching airfoil at time t is given by

$$\alpha(t) = \alpha_m + 4.2 \sin\left(2kM_\infty t + \tfrac{3}{2}\pi\right) \tag{1}$$

where α_m is the mean angle of pitch and t is the time step nondimensionalized by chord and freestream speed of sound. The study considered three mean angles of pitch of $\alpha_m = 4$, 11, and 15 deg, corresponding to attached flow, light dynamic stall, and deep dynamic stall, respectively. The phase shift $\frac{3}{2}\pi$ makes unsteady computations begin at the lowest angle of attack of a pitching cycle with zero angular velocity.

After investigating the sensitivity of the computations to grid density, time step, and size and number of subiterations at each time step, final computations were made on a C-type 259×60 grid: 100 points on the upper surface and 80 points on the lower surface of the airfoil, 40 points along the wake cut, minimum wall normal spacing of $\Delta z = 0.0001$ (0.0004 for the k–ϵ model) chord, and the far-field boundary located at 15 chord lengths away from the airfoil. Time marching is achieved using a time step size of $\Delta t = 0.0113$, which corresponds to 10,000 time steps per pitching cycle. At each time step, three subiterations were used to reduce numerical errors from approximate factorization of the implicit scheme.

Figures 1 and 2 show the hysteresis of lift, drag, and pitching moment coefficient for attached flow and light dynamic stall, respectively. The measured force coefficients were obtained from pressure data only, i.e., the contribution from viscous wall shear stress was not included. In about half of a cycle after the initiation of unsteady computations, the hysteresis of force coefficients start to show fully periodic behavior in both cases. In general, the computed force coefficients agree well with the experimental data during the upstroke for both flows.

Figure 1 shows predictions compared with measurements for the attached flow case. Although the flow is simple, there is enough boundary-layer thickening to make it difficult to predict the hysteresis of the force coefficients accurately. The predictions by the S–A and the k–ϵ models agree very well with the measured data for all three force coefficients. The B–L model shows fairly good agreement with the measurements for C_l and C_d but not for C_m.

In light dynamic stall, shown in Fig. 2, the flow separates near the trailing edge as the airfoil pitches up, and this separation disappears as the airfoil pitches down. Because the light dynamic stall is sensitive to the onset of separation, it is a good test case for evaluating turbulence models. The B–L model performs poorly in predicting all three force coefficients. The thin envelope of the C_l hysteresis curve by the B–L model indicates that the model does not give separation during the oscillatory cycle. The k–ϵ model shows excellent agreement with the measured C_l whereas the S–A model shows a little underprediction during the downstroke. For the drag and moment coefficients, the S–A and the k–ϵ models show comparable agreement with the experimental data.

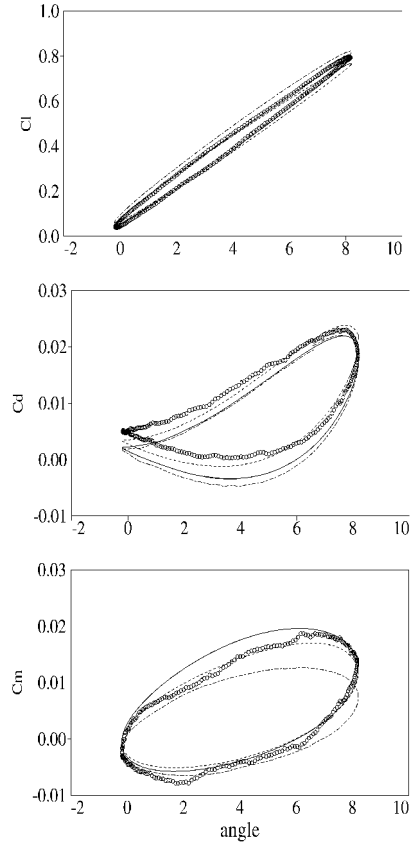

Fig. 1 Hysteresis of lift, drag, and pitching moment for attached flow of an oscillating NACA 0015 airfoil at α (deg) = 4 + 4.2 sin($2kM_\infty t$ + 1.5π), M_∞ = 0.29, Re = 1.95 × 10^6, k = 0.1: ——, S–A; – – –, B–L; – – –, k–ϵ; and ○ experiment.

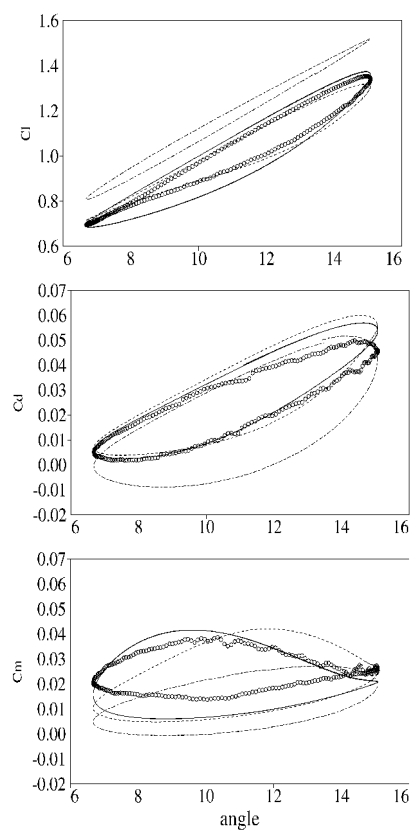

Fig. 2 Hysteresis of lift, drag, and pitching moment for light dynamic stall of an oscillating NACA 0015 airfoil at α (deg) = 11 + 4.2 sin($2kM_\infty t$ + 1.5π), M_∞ = 0.29, Re = 1.95 × 10^6, k = 0.1: ——, S–A; – – –, B–L; – – –, k–ϵ; and ○ experiment.

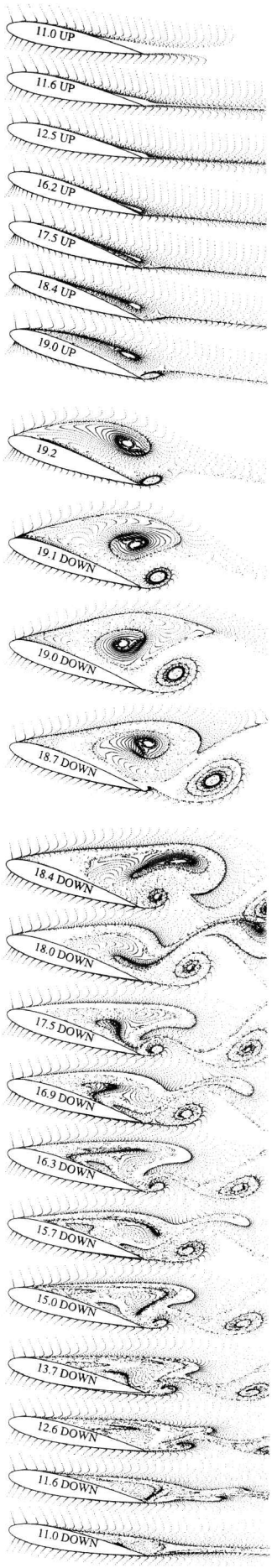

Fig. 3 Particle tracing of oscillating NACA0015 airfoil: α (deg) = 15 + 4.2 sin($2kM_\infty t + 1.5\pi$), M_∞ = 0.29, Re = 1.95 $\times$ 10^6, and k = 0.1.

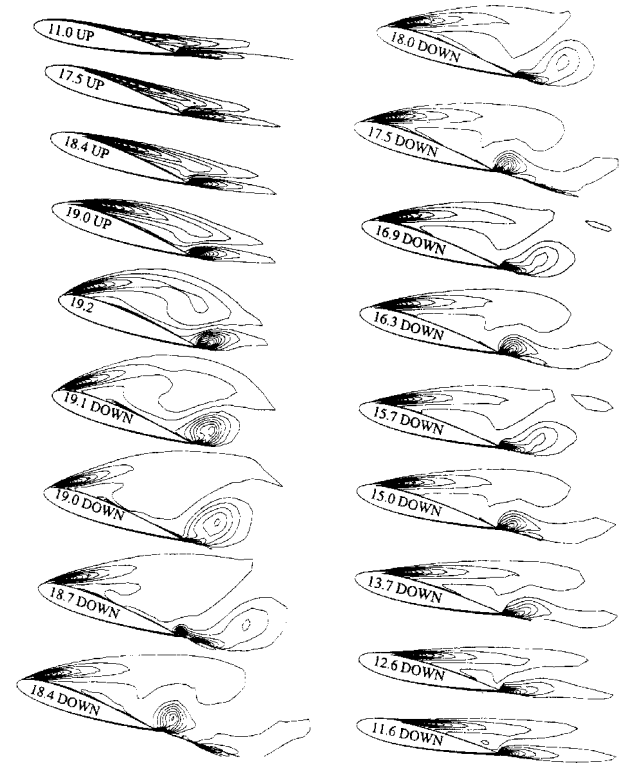

Fig. 4 Vorticity contours for oscillating NACA 0015 airfoil: α (deg) = 15 + 4.2 sin($2kM_\infty t + 1.5\pi$), M_∞ = 0.29, Re = 1.95 $\times$ 10^6, and k = 0.1.

The computed deep-stall hysteresis loops of the force coefficients (not shown) are less satisfactory, and they can only be considered semiquantitative on the downstroke. However, Fig. 3 shows a series of instantaneous pictures of computed streaklines of the deep dynamic stall case. During the second cycle of computation with the S–A model, solutions and grids at 600 intermediate time steps were saved for computing the streaklines. The computation was done by the unsteady flow analysis toolkit (UFAT).[10] At each time step, new particles are released from two near-leading-edge stations: one on the upper and the other on the lower surface of the airfoil. Then UFAT follows these particles, revealing a Lagrangian description of flow phenomena.

Figure 4 shows a series of calculated vorticity contours for the deep dynamic stall case. According to the calculations, the vorticity of the flowfield varies widely from zero to a few thousand. The large-scale vortices observed in Fig. 3 have low vorticity in the order of one while vorticity greater than 10 is limited to the wall region near the leading edge. Therefore, the vorticity contour levels ranging from 0 to 10 is used. In this way, the evolution of large-scale vortices can be captured without losing the global picture of the flow structure. The vorticity near the leading edge of the upper surface is the most intense due to the flow acceleration along the curved leading edge of the upper surface. During the whole cycle, the vorticity contours give the overall appearance of remaining attached to the leading and trailing edges. Only their size and thicknesses vary as the airfoil pitches up and down.

Acknowledgment

The investigation is supported by the U.S. Army Aeroflightdynamics Directorate at the NASA Ames Research Center.

References

[1] Baldwin, B. S., and Lomax, H., "Thin Layer Approximation and Algebraic Model for Separated Turbulent Flows," AIAA Paper 78-257, Jan. 1978.

[2] Spalart, P. R., and Allmaras, S. R., "A One-Equation Turbulence Model for Aerodynamic Flows," AIAA Paper 92-0439, Jan. 1992.

[3] Jones, W. P., and Launder, B. E., "The Prediction of Laminarization with a Two-Equation Turbulence Model," *International Journal of Heat and Mass Transfer*, Vol. 15, Feb. 1972, pp. 301–314.

[4]Srinivasan, G. R., Baeder, J. D., Obayashi, S., and McCroskey, W. J., "Flowfield of a Lifting Rotor in Hover: A Navier–Stokes Simulation," *AIAA Journal*, Vol. 30, No. 10, 1992, pp. 2371–2378.

[5]Roe, P. L., "Approximate Riemann Solvers, Parameter Vectors, and Difference Schemes," *Journal of Computational Physics*, Vol. 43, No. 2, 1981, pp. 357–372.

[6]Yoon, S., and Kwak, D., "Implicit Navier–Stokes Solver for Three-Dimensional Compressible Flows," *AIAA Journal*, Vol. 30, No. 11, 1992, pp. 2653–2659.

[7]Patankar, S. V., *Numerical Heat Transfer and Fluid Flow*, Hemisphere, New York, 1980, pp. 48, 49.

[8]Chen, C.-L., and McCroskey, W. J., "Numerical Simulation of Helicopter Multi-Bladed Rotor Flow," AIAA Paper 88-0046, Jan. 1988.

[9]Piziali, R. A., "2-D and 3-D Oscillating Wing Aerodynamics for a Range Angles of Attack Including Stall," NASA TM-4632, Sept. 1994.

[10]Lane, D. A., "UFAT—A Particle Tracer for Time-Dependent Flow Fields," *Proceedings of Visualization '94* (Washington, DC), IEEE Computer Society, 1994, pp. 257–264.

A. Plotkin
Associate Editor

Freestream Parameter Estimation Using Heat Flux Measurements

A. K. Alekseev*
RSC ENERGIA, Korolev,
Moscow Region 141070, Russia

Nomenclature

e	= specific energy, $C_v T$
f	= flow parameters (ρ, U, V, T)
P	= pressure
Q	= heat flux
Re	= Reynolds number
T	= temperature
t	= time
U	= velocity
X, Y	= coordinates
μ	= viscosity

Subscripts and Superscripts

comp	= computation
exp	= experiment
w	= wall conditions
∞	= freestream parameters

Introduction

WHEN it is necessary to determine flow parameters governing heat transfer, the need to solve inverse convection problems arises. For example, determining the boundary heat flux using temperature measurements at another boundary is discussed by Moutsoglou[1] for a two-dimensional region with steady-state flow described by the Navier–Stokes equations. Estimation of freestream parameters is of practical importance in many problems. Direct measurement of these parameters is accompanied by certain technical difficulties caused, for example, by flowfield distortion or the heat flux acting on the sensor. Wall temperature measurements are the simplest from this viewpoint.

The estimation of free flow parameters using heat flux measurements at different points at body surface is considered. Let us consider the supersonic gas flow described by equations of viscous compressible gas (Navier–Stokes). The set of freestream parameters governs heat flux distribution along the surface (along the X coordinate):

$$(\rho_\infty U_\infty T_\infty) \longrightarrow [Q_w(X_1),\ Q_w(X_2),\ Q_w(X_3)] \tag{1}$$

We seek to determine ρ_∞ U_∞ and T_∞ using heat flux measurements $Q_w(X_j)$ as the input data. We shall minimize the discrepancy between computed and experimental values of $Q_w(X_j)$, i.e.,

$$\varepsilon(\rho_\infty U_\infty T_\infty) = \sum_j \left[Q_w^{\exp}(X_j) - Q_w^{\text{comp}}(X_j) \right]^2 \tag{2}$$

The mathematical model consists of a flowfield solver and an optimization algorithm minimizing the discrepancy of computed and experimental data by varying the boundary conditions.

The Jacoby matrix $A_{ij} = \partial Q(X_i)/\partial f_j$ for the transformation $(\rho, T, U) \longrightarrow Q(X_1, X_2, X_3)$ is studied for the singularity search:

$$A_{ij} = \frac{\partial Q(X_i)}{\partial f_j} = \begin{bmatrix} \dfrac{\partial Q(X_1)}{\partial \rho} & \dfrac{\partial Q(X_1)}{\partial U} & \dfrac{\partial Q(X_1)}{\partial T} \\ \dfrac{\partial Q(X_2)}{\partial \rho} & \dfrac{\partial Q(X_2)}{\partial U} & \dfrac{\partial Q(X_2)}{\partial T} \\ \dfrac{\partial Q(X_3)}{\partial \rho} & \dfrac{\partial Q(X_3)}{\partial U} & \dfrac{\partial Q(X_3)}{\partial T} \end{bmatrix} \tag{3}$$

The determinant is identically equal to zero in the following events (global singularity). 1) The flowfield is determined not by the total parameter space $(\rho_\infty U_\infty T_\infty)$ but by some subspace of the lower dimension, for example, $(Re_\infty M_\infty)$. 2) The heat flux $Q_w(t, X)$ is determined not by total space of flow parameters but by some subspace of lower dimension. 3) The spatial heat flux variation $Q_w(X)$ is multiplicative along the X coordinate: $Q_w(X) = Q_w(X_0)F(X/X_0)$, i.e., the heat flux is self-similar along X.

The computation of the matrix A determinant allows one to consider the singularity only locally in regard to the flow parameters because of the problem nonlinearity. A global singularity can be detected by means of the Lie group. In particular, the transformation $Q(X) = Q(X_0, \rho_\infty U_\infty T_\infty)\varphi(X/X_0)$ corresponds to the Navier–Stokes equations invariance relative the operator $B = \eta(\rho_\infty U_\infty T_\infty)\partial/\partial X$. This operator is absent in the set of the Lie group basis of the Navier–Stokes equations that provides the absence of this type of singularity. Nevertheless, the transformation $Q(X) = Q(X_0, \rho_\infty U_\infty T_\infty)\varphi(X/X_0)$ can take the place for an infinitely thin boundary layer. Thus, although the matrix (3) is nonsingular, it can be very close to a singular one that causes instability.

A global singularity exists for special events and can be easily detected by computations. The most practical interesting problem arises when a global singularity is absent. In that event, the nonlinearity of the problem becomes crucial. $Q_w(t, X)$ nonlinearly depends on $(\rho_\infty U_\infty T_\infty)$ and nonlinearly varies along X. Then, there is a six parameter local transformation: $(X^3 \times f^3) \times f^3 \longrightarrow Q^3$. If this transformation is smooth and if f^3 and Q^3 are smooth manifolds, then, according to the Sard theorem,[2] such a transformation should be nonsingular (in the common case). If $\det[\partial Q(X_i)/\partial f_j]$ is not identical to zero, the set of points $X \in R^3$ for which $\det[\partial Q(X_i)/\partial f_j] = 0$ is either empty or a smooth two-dimensional surface embedded into R^3 space. It can be easily seen that f^3 and Q^3 are smooth manifolds, and the transformation is smooth for flows considered here (having no shocks on the surface). Thus, the problem [Eq. (1)] will be nonsingular with the probability close to 1.

These speculations lead to the conclusion that, if the numerical experiments have demonstrated nonsingularity in some point, the problem is nonsingular in a significant part of the phase space.

A number of difficulties arise at the investigation of the Navier–Stokes problem, in general, which are connected with the need for repeated solution of the direct problem and large computation time. In this connection, the two-dimensional spatially evolutional flows that can be solved with quick marching methods are of special interest. The supersonic flow over a flat plate with a compression corner was considered. The flowfield was computed using the parabolized Navier–Stokes (PNS) method. The finite difference method with second-order accuracy in the Y direction (symmetrical differences with fourth-order smoothing) and first order in X was used. At every

Received May 14, 1996; revision received March 31, 1997; accepted for publication April 3, 1997.

*Senior Researcher, Department of Aerodynamics and Heat Transfer.